Visualization of vitamin A metabolism

Koenders, S.T.A.

Chapter 5

Comparative and Competitive ABPP of ALDHs in Breast Cancer Cells using LEI-945

Published as part of S.T.A. Koenders *et al., ACS Cent. Sci.*, **5**, 1965-1974 (2019).

Introduction

Aldehyde dehydrogenases (ALDHs) play an important role in the detoxification of the cellular environment. It is therefore not surprising that an upregulation of ALDH activity in breast cancer cells has been linked with chemo- and radiotherapy resistance.[1] For example, the presence of ALDH1A1 has been found to correlate with resistance in cancer tissue towards cyclophosphamide and the expression of ALDH1A3 is associated with poor clinical outcome in breast cancer.[2–6] Noteworthy, ALDH1A1 and ALDH1A3 have also been reported as biomarkers for cancer stem cells.[7]

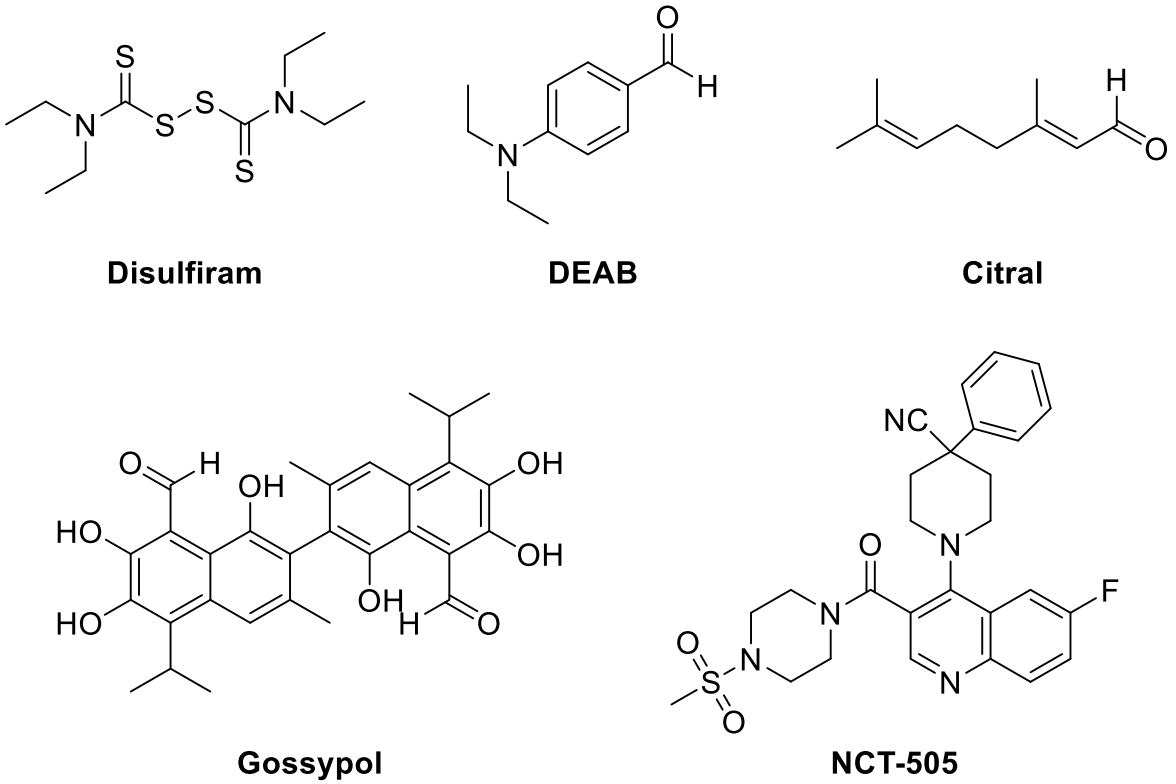

Fig. 5.1 | Chemical structures of ALDH inhibitors disulfiram, DEAB, citral, gossypol and NCT-505.

Inhibition of these ALDHs is therefore a potential therapeutic strategy to overcome drug resistance in cancer. The activity of these enzymes is currently measured using the fluorescence-activated cell sorting (FACS) based ALDEFLUOR assay, which reports on global ALDH activity.[8] It uses a fluorescent aldehyde that upon oxidation to a charged carboxylate is trapped within the cell. The ALDEFLUOR assay does not, however, discriminate between individual ALDHs. Selective ALDH inhibitors are required to study the physiological role of ALDHs in cancer cells in an acute and dynamic matter. Such inhibitors may serve as potential drug candidates. Reported ALDH inhibitors, such as disulfiram, 4-diethylaminobenzaldehyde (DEAB), citral and gossypol, however, are weakly active and/or demonstrate promiscuous behaviour, which complicates the interpretation of their biological effects.[9,10] Recently, NCT-505 was developed as the first potent ALDH1A1 inhibitor with a >1000-fold selectivity over ALDH1A3 as determined in a biochemical assay.[11] NCT-505 was cytotoxic to ovarian cancer cells and sensitized them to paclitaxel. The cellular selectivity profile and mode-of-action of NCT-505 has not been reported yet, and knowledge hereof would be of importance to guide its therapeutic development. As well, the determination of target protein engagement and off-target activities of small molecules is an essential step in drug discovery.

This chapter describes mapping of ALDH activity in breast cancer cells using comparative ABPP using the first-in-class retinal-based **LEI-945**.[12] Competitive activity-based protein profiling (ABPP) using **LEI-945** was employed to determine the cellular target engagement and selectivity profile of NCT-505 in MDA-MB-468 breast cancer cells. Both ALDH1A1 and ALDH1A3 were inhibited by NCT-505 resulting in an overall reduced cell viability. Following establishment of the selectivity profile of NCT-505, live cell imaging was performed to study the physiological effects of ALDH inhibition in cancer.

Results

LEI-945 reveals distinct ALDH activities in cells of different breast cancer subtypes

To determine whether **LEI-945** can be used to profile the activities of these ALDHs in breast cancer cell lines, a panel of seven breast cancer cells was selected ranging from aggressive basal origin (MDA-MB-231, BT-20, MDA-MB-468 and HCC38) to less aggressive luminal origin (SK-BR-7, MCF7 and SK-BR-3).[13] Their general ALDH activity was measured using the ALDEFLUOR assay.[14]

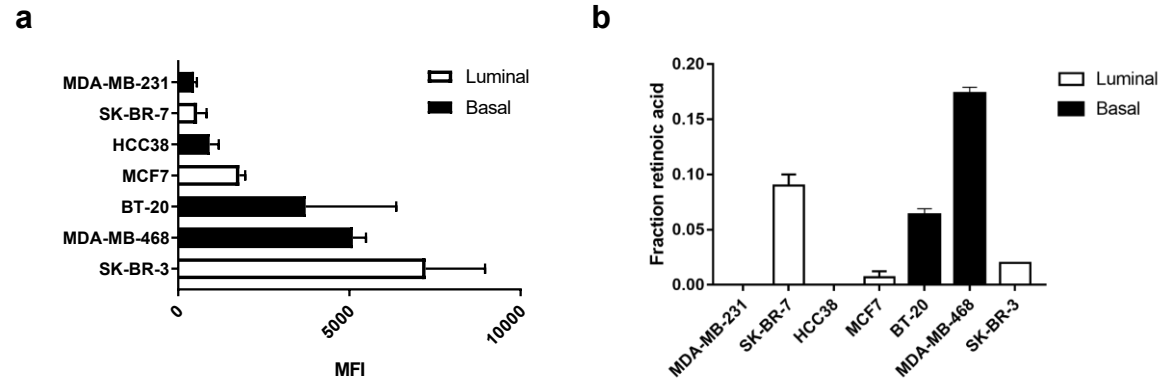

Fig. 5.2 | ALDH activity in breast cancer cells. a, Mean fluorescence intensity (MFI) of ALDH activity measured in breast cancer cell lines using the ALDEFLUOR assay. Data are represented as mean values ± SD; $N = 3$ independent experiments with each $n = 3$ experiments per group (biological replicates). **b**, Retinoic acid production by breast cancer cell lines. Data represent mean values ± SD; $N = 3$ experiments (biological replicates) measured twice.

Based on this assay the breast cancer cell lines were divided in two groups: ALDH^{low} (MDA-MB-231, SK-BR-7, HCC38 and MCF7) and ALDH^{high} (BT-20, MDA-MB-468 and SK-BR-3) (**Fig. 5.2b, Supplementary Fig. 5.1**). These two groups did not correlate with the breast cancer subtype.

Next, the capability of the breast cancer cell lines to convert retinal into retinoic acid was determined by liquid chromatography/mass spectrometry. Retinal (10 μM, 1 h)-treated cells were lysed and the lipids extracted after which the unique UV absorption of the retinoids relative to other metabolites was used to determine to which extent retinal was converted (**Fig. 5.2b**). The results of the ALDEFLUOR assay (**Fig. 5.2a**) did not correlate with the ability of cells to produce retinoic acid. For example, while MDA-MB-468 and SK-BR-3 were both classified as $ALDH^{high}$, only MDA-MB-468 cells produced significant amounts of retinoic acid.

To determine whether ABPP using **LEI-945** would be able to explain these apparent contradictory results by determining the levels of active aldehyde dehydrogenases in each breast cancer cell line, chemical proteomics experiments were performed with samples from all seven breast cancer cell lines using **LEI-945** (1 μM, 1 h) (**Fig. 5.3a**). ALDH1A1 was found in SK-BR-7 and MDA-MB-468. ALDH1A3 was detected in BT-20, MDA-MB-468 and SK-BR-3. ALDH2 was significantly enriched in MDA-MB-231, HCC38, MDA-MB-468 and SK-BR-3. ALDH3A2 was identified in MDA-MB-231, SK-BR-7, BT-20, MDA-MB-468 and SK-BR-3.

Comparison of the chemical proteomics data with data from transcriptomics and global proteomics experiments of these breast cancer cell lines revealed in general a high correlation with r of 0.80 and 0.74 between enzyme activity and mRNA and protein levels, respectively (**Fig. 5.3b,c**). Levels of active ALDH1A1 and ALDH1A3 enzymes were higher than expected on the basis of the mRNA and protein levels, indicating that the activity of these enzymes is potentially regulated post-translationally, as was previously reported.[15,16]

Active ALDH1A1 was most abundant in the MDA-MB-468 cells, whereas SK-BR-3 had high levels of active ALDH2 and no discernible levels of active ALDH1A1. Since human ALDH2 does not convert retinal into retinoic acid[17], but is an efficient oxidizer of numerous aldehydes, these data may explain the discrepancy between the ALDEFLUOR assay and the retinal conversion assay. Taken together, this data shows that **LEI-945** has the ability to identify individual ALDH isozyme activities in cancer cells and report on the well-known cancer biomarkers ALDH1A1 and ALDH1A3.[7]

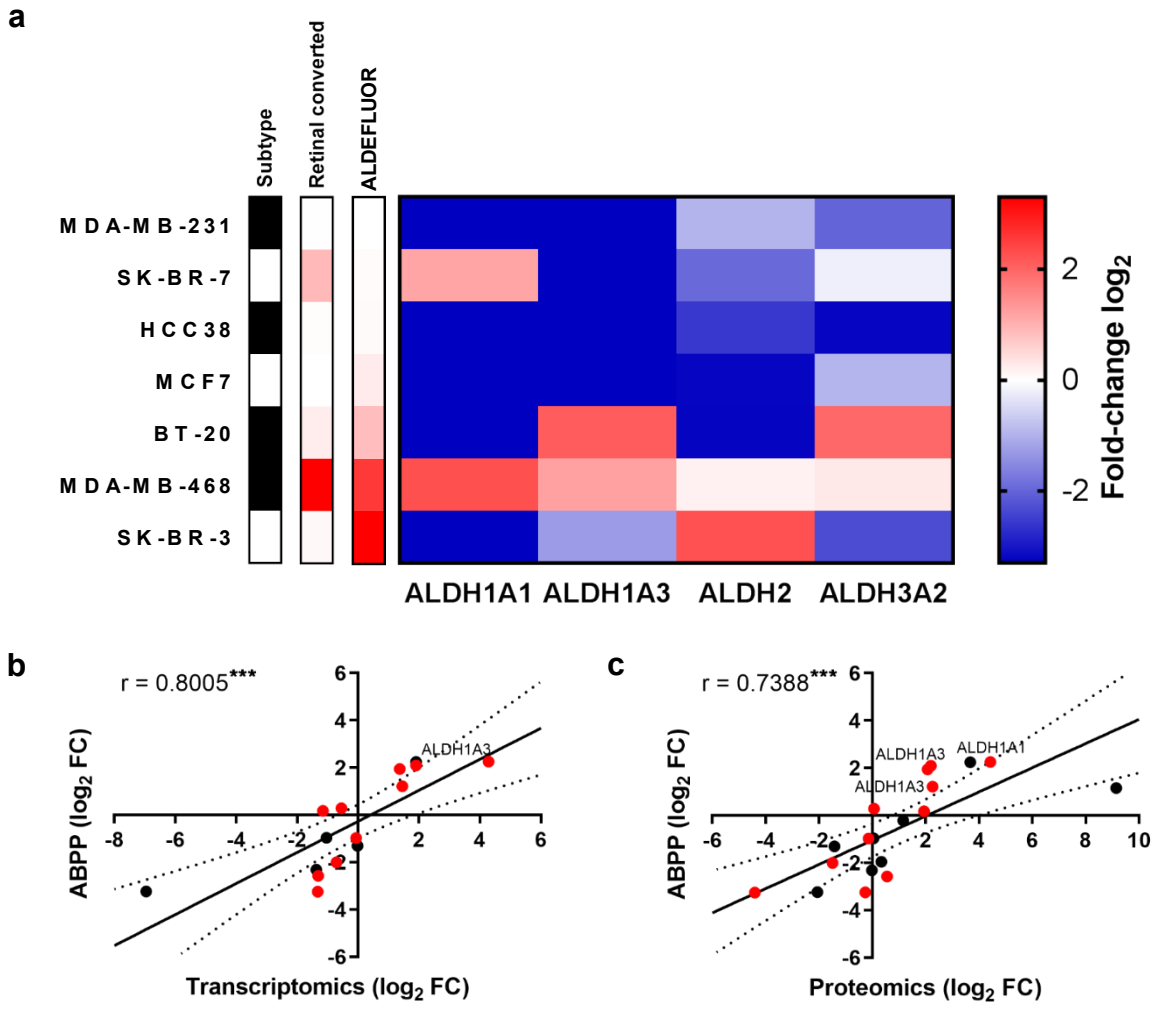

Fig. 5.3 | Profiling levels of active ALDH enzymes in breast cancer cell lines. a, ALDH profiling of breast cancer cell lines using chemical proteomics. The subtype column indicates if the cell line belongs to the luminal subtype (white) or basal subtype (black). The retinal converted column shows the amount of retinal converted to retinoic acid over 4 h in a gradient from 0% (white) to 100% (red). The ALDEFLUOR column shows the ALDH activity as determined by the ALDEFLUOR assay in a gradient from low (white) to high (red). The heatmap shows the fold-change in LFQ value for each ALDH enzyme compared to the average for each ALDH enzyme. $N = 2$ independent experiments with each at least $n = 3$ experiments per group (biological replicates). **b**, Correlation of transcriptomics data with ABPP data. ALDHs measured in cell lines with a basal subtype are shown as red dots and the ones with a luminal subtype are shown as black dots and the Pearson's correlation reported for the correlation between ABPP and transcriptomics, ($r = 0.8005$; $p = 0.0003$). **c**, Correlation of proteomics data with ABPP data. ALDHs measured in cell lines with a basal subtype are shown as red dots and the ones with a luminal subtype are shown as black dots and the Pearson's correlation reported for the correlation between ABPP and proteomics, ($r = 0.7388$; $p = 0.0003$).

NCT-505 inhibits ALDH1A1 and ALDH1A3 in MDA-MB-468 cells

For successful drug discovery it is advantageous to understand the molecular and cellular mode-of-action of a drug candidate. So far, studies on the physiological effects of ALDH inhibition in cancer have been mostly performed with poorly active and/or promiscuous inhibitors, which have not been properly characterized in biological systems.[1,10,18–20] This complicates the interpretation of the physiological function ascribed to a specific ALDH. Here, **LEI-945** was used to study the cellular ALDH interaction profile of the ALDH1A1 inhibitor NCT-505. First, it was confirmed that NCT-505 was able to significantly reduce cell viability and proliferation of MDA-MB-468 cells, which expressed the highest levels of ALDH1A1 (**Fig. 5.4a,b**).

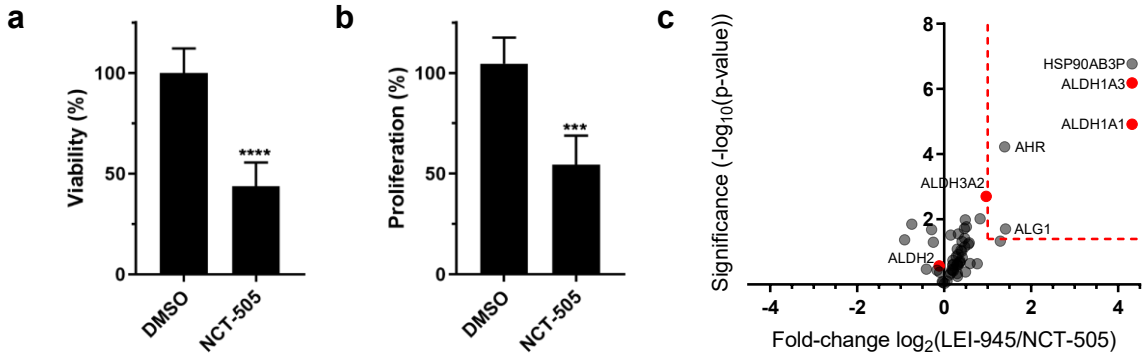

Fig. 5.4 | Target engagement studies of NCT-505 in MDA-MB-468 cells. **a**, Cell viability of MDA-MB-468 cells after treatment with NCT-505 (30 µM) for 72 h. **b**, Cell proliferation of breast cancer cell lines after treatment with NCT-505 (30 µM) for 72 h. For parts **a** and **b**, data represent mean values ± SD; $N = 3$ biological replicates with each $n = 3$ experiments per group. ***P < 0.001; ****P < 0.0001; *t* test, two sided. **c**, Volcano plot of *in situ* competitive ABPP experiment in MDA-MB-468 to determine off-targets of ALDH inhibitor NCT-505 (30 µM). $N = 4$ experiments per group (biological replicates).

To determine the cellular target engagement and off-target activities, a chemical proteomics experiment with **LEI-945** was performed using MDA-MB-468 cells *in situ* treated with NCT-505. This competitive ABPP experiment showed that both ALDH1A1 and ALDH1A3 were inhibited by NCT-505 at the concentration used in the cell viability and proliferation assay (**Fig. 5.4c**). Putative heat shock protein HSP 90-β-3 (HSP90AB3P), the aryl hydrocarbon receptor (AHR) and chitobiosyldiphosphodolichol β-mannosyltransferase (ALG1) were also identified as off-targets of NCT-505.

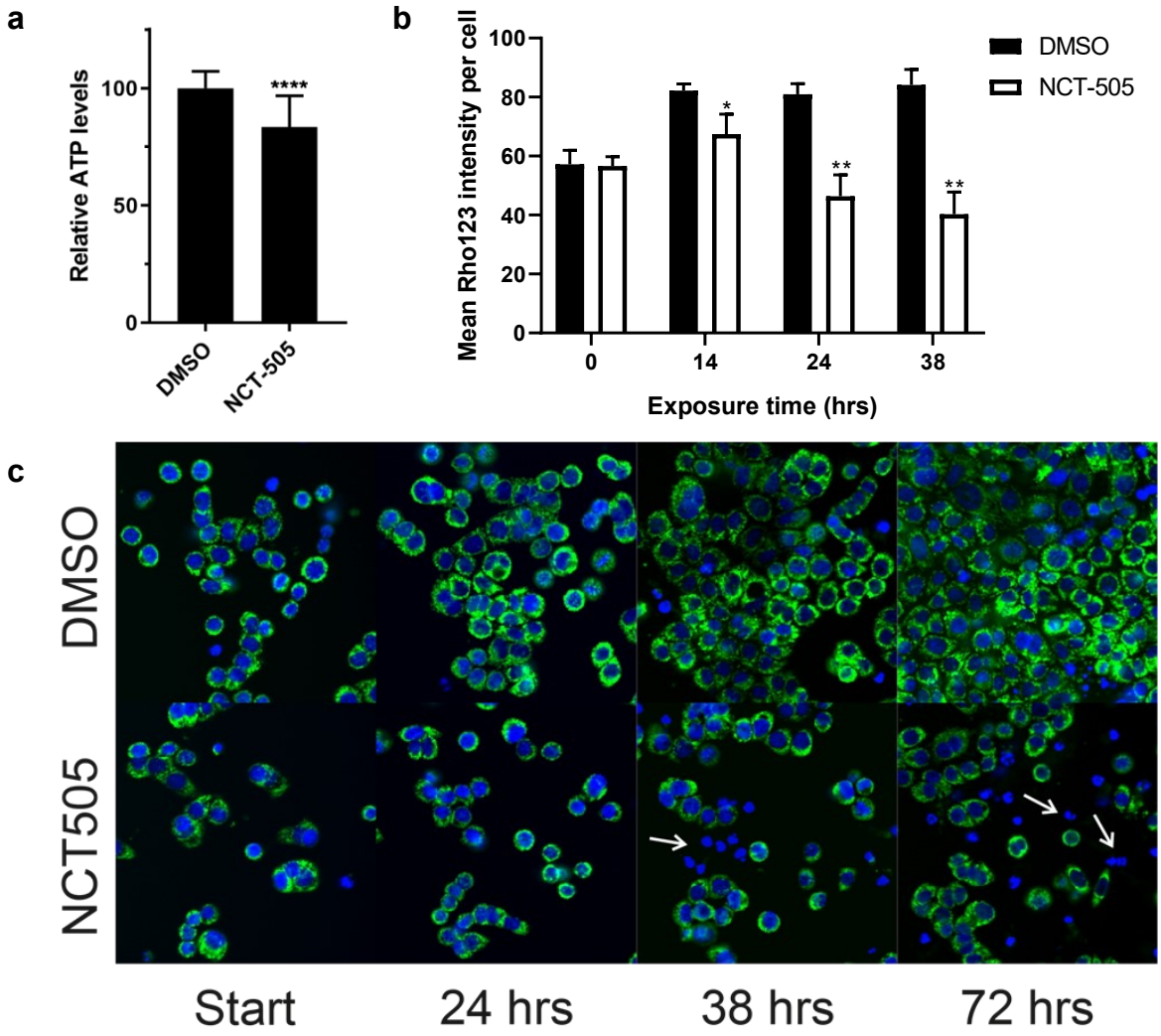

Fig. 5.5 | Impact of NCT-505 on mitochondrial function. a, Relative ATP levels of vehicle and NCT-505 (30 μM)-treated MDA-MB-468 cells as determined by CellTiter-Glo assay. Data represent mean values ± SD; $N = 3$ biological replicates with each $n = 3$ experiments per group. ****P < 0.0001. **b**, Relative mitochondrial membrane potential ($\Delta\Psi_m$) of vehicle and NCT-505 (30 μM)-treated MDA-MB-468 cells visualized by rhodamine 123 and measured over time. Data represent mean values ± SD; $N = 3$ biological replicates with each 5 experiments per group. **P < 0.01; *t* test, two sided. **c**, Representative images of time-lapses performed by confocal microscopy of mitochondrial potential. Mitochondrial membrane potential was visualized using rhodamine 123 dye (green) while the nuclei were detected with live Hoechst (blue). Arrows indicate dying cells without rhodamine signal.

Having established the cellular aldehyde dehydrogenase interaction profile of NCT-505 by ABPP using **LEI-945**, the biological effect of this dual ALDH1A1/ALDH1A3 inhibitor in MDA-MB-468 cells was further characterized by studying its effects on mitochondrial function, cell cycle and cell death. NCT-505 produced a limited, but significant, reduction in adenosine triphosphate (ATP) levels (**Fig. 5.5a**).

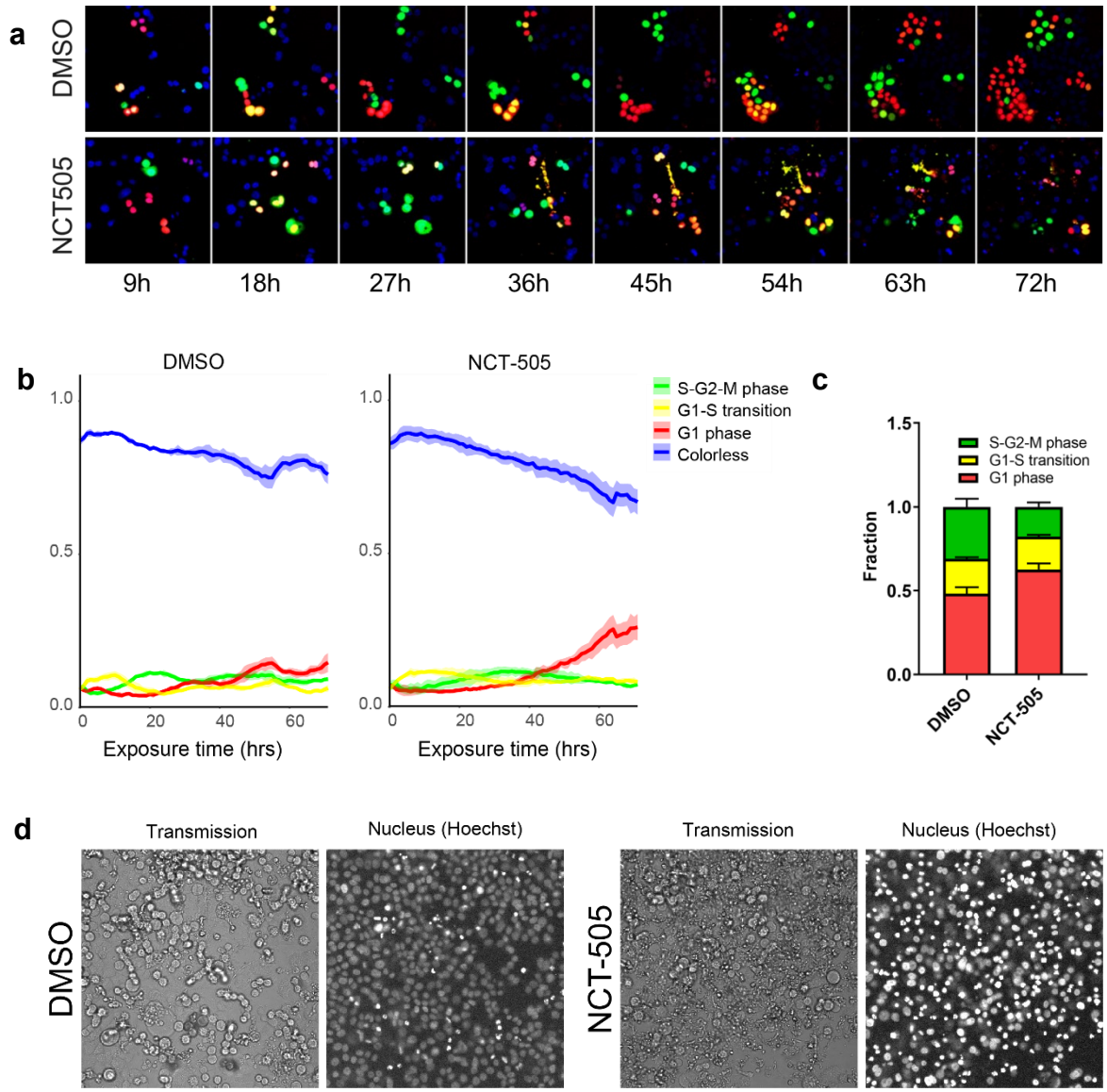

Fig. 5.6 | NCT-505 arrests cells in the G1 phase. a, Representative images of FUCCI-expressing MDA-MB-468 cells. Cell cycle phases were visualized by FUCCI expression: G1 phase (red), G1-S transition (yellow) and S-G2-M phase (green). The nuclei were detected with live Hoechst (blue). **b**, FUCCI analysis of the cell cycle using time-lapse microscopy. MDA-MB-468 FUCCI cells were treated with NCT-505 (30 µM) for 72 h and imaged every hour. **c**, Distribution over the different cell cycle phases of vehicle and NCT-505 (30 µM)-treated FUCCI-expressing MDA-MB-468 cells after 72 h. Data represent mean values ± SD; $N = 3$ biological replicates with each 5 experiments per group. **d**, Representative images of nuclei condensation. MDA-MB-468 cells were treated with NCT-505 (30 µM) for 72 h. Hoechst staining showed highly condensed nuclei in the NCT-505-treated cells compared to vehicle.

Mitochondrial membrane potential ($\Delta\Psi_m$) upon preincubation of MDA-MB-468 cells was also reduced as assessed with rhodamine 123, a fluorescent marker for mitochondrial activity, suggesting that mitochondrial function was altered (**Fig. 5.5b,c**).

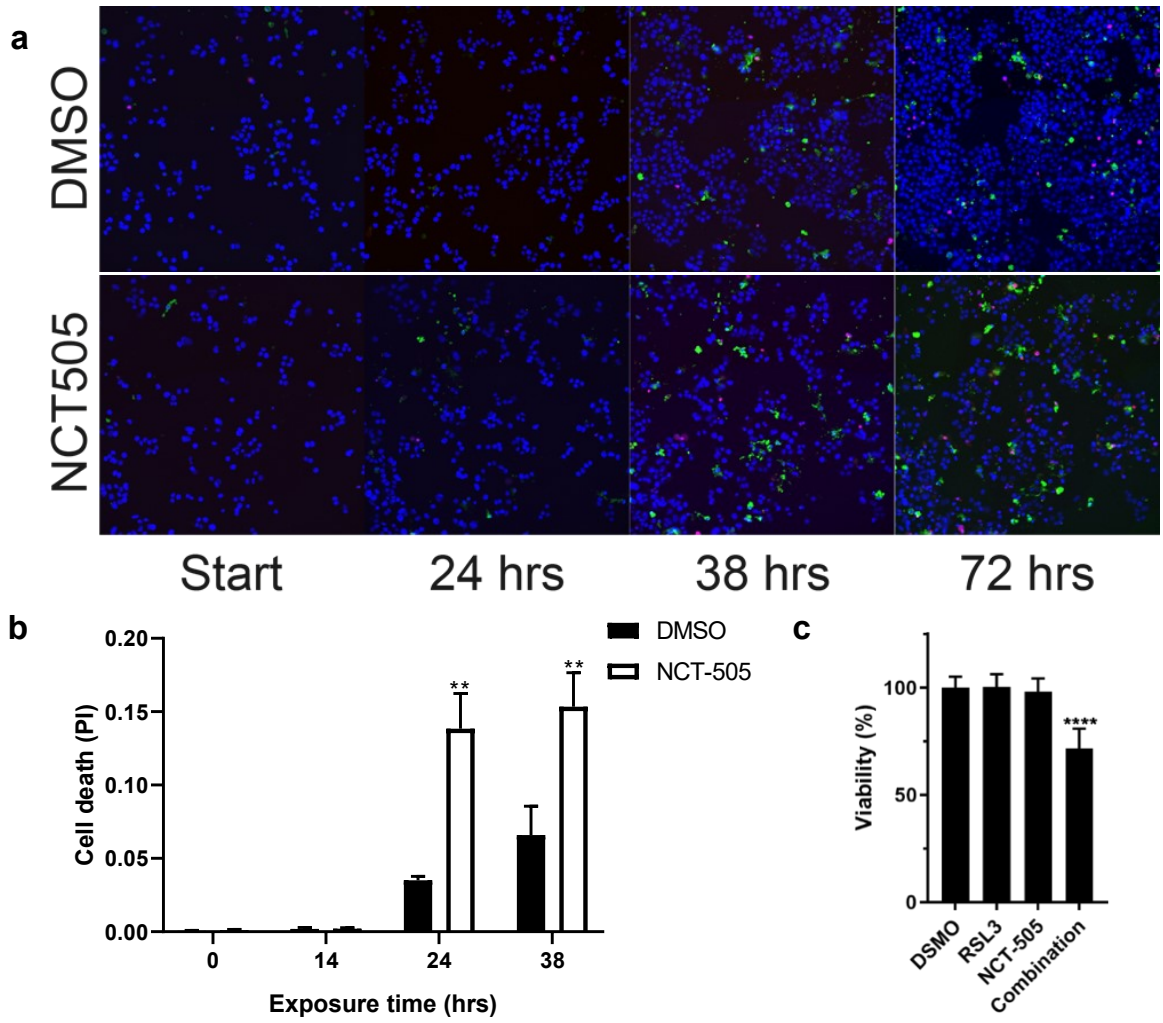

Fig. 5.7 | ALDH1A1/1A3 inhibition cells undergo non-apoptotic cell death. a, Representative images of time-lapses performed by confocal microscopy of cell death. MDA-MB-468 cells were treated with NCT-505 (30 µM) for 72 h. Cell death was visualized using propodium iodide (PI; red), Annexin V (AnV; green) and the nuclei were detected with live Hoechst (blue). **b**, Cell death profile of vehicle and NCT-505 (30 µM)-treated MDA-MB-468 cells as determined by propidium iodide (PI) staining and measured over time. Data represent mean values ± SD; $N = 3$ biological replicates with each 5 experiments per group. **P < 0.01; *t* test, two-sided. **c**, Synergy between RSL3 (30 nM) and NCT-505 (3 µM) measured using a viability assay after 72 h of treatment. Data represent mean values ± SD; $N = 3$ biological replicates with each 6 experiments per group. ****P < 0.0001.

In addition, exposure to NCT-505 arrested cells in the G1 cycle as determined by fluorescent ubiquitination-based cell cycle indicators (FUCCI) (**Fig. 5.6a,b,c**).[21] The nuclei of the NCT-505-treated cells were highly condensed compared to vehicle-treated cells indicating dying cells, which had no rhodamine 123 signal as well (**Fig. 5.6d, see arrows in Fig. 5.5c**). A significant increase in the fraction of propidium iodide (PI) positive cells was observed in NCT-505-treated cells, which suggested that the cells underwent necrosis (**Fig. 5.7a,b**).

As changes in mitochondrial morphology are a distinctive feature of ferroptosis[22], the observed non-apoptotic cell death in combination with alterations in mitochondrial function might indicate that the dying cells undergo ferroptosis. To determine whether incubation with RSL3, a compound that induces ferroptosis via inhibition of GPX4[23,24] and inhibition of ALDH1A1/ALDH1A3 could synergistically induce cell death, MDA-MB-468 cells were treated with ineffective, low concentrations of GPX4 inhibitor RSL3 (30 nM) or NCT-505 (3 μM). At these concentrations, the inhibitors did not show any reductions in cell viability, whereas the combination led to a significant decrease in cell viability with a combination index value of 0.87 indicating synergy (**Fig. 5.7c**).

Discussion

LEI-945 was able to detect and compare individual active ALDH isozymes in breast cancer cell lines. The ALDH profiles generated using **LEI-945** could be used to explain the ability of certain cell lines to produce retinoic acid, where the ALDEFLUOR assay could not. It also detected levels of active ALDH1A1 enzyme in the SK-BR-7 cell line, while the ALDEFLUOR assay reported no ALDH activity. This method can also be used in combination with the ALDEFLUOR assay by sorting cells based on global ALDH activity and subsequently subjecting the sorted cell populations to comparative ABPP analysis. Thus providing both qualitative and quantitative information on the levels of active ALDH enzymes in therapy-resistant cancer (stem) cells enabling a better mechanistic understanding of the underlying biology, which is ALDH isozyme dependent.[25]

Furthermore, **LEI-945** enabled target engagement and cellular selectivity studies of the recently reported ALDH1A1 inhibitor NCT-505. This ABPP method revealed that NCT-505 does not only inhibit ALDH1A1, but also ALDH1A3, at concentrations that significantly reduced cell viability and proliferation of MDA-MB-468 cells via inhibition of mitochondrial function, cell cycle arrest in the G1 phase and necrosis-induced cell death. The concentration used in this study is in accordance with the reported EC_{50} value derived from OV-90 ovarian cancer cells grown in 2D cell culture.[11] Maloney *et al*. showed an increase in sensitivity towards NCT-505 when cells are grown in 3D cell culture, possibly due to the accompanying elevated levels of ALDH1A1 expression.[11] Elevated ALDH expression in 3D cell culture compared with 2D has also been described by others.[26,27] This phenomenon could be studied in more depth by looking at changes in the levels of active enzymes using **LEI-945**.

Ferroptosis induced via GPX4 inhibition was synergistic with NCT-505-mediated toxicity. This combined therapy is of interest as both therapeutic targets, GPX4 and ALDH1A1, have been linked to therapy resistance in cancer.[20,23,24] Since both enzymes are involved in the detoxification of lipid peroxidation products, this might explain the observed synergistic effect.[28–30] Since NCT-505 also inhibits ALDH1A3, this data does not rule out the possibility that ALDH1A3 may be an interesting drug target to tackle drug resistance in cancer.

Conclusion

To conclude, **LEI-945** can be used for comparative and competitive ABPP of cancer cells and ALDH inhibitors, thereby providing guidance in the target validation and discovery of cancer (stem) cell-based therapies. Thus, these results showcase the application of substrate-based probes in interrogating pathologically relevant enzyme activities. They also highlight the general power of chemical proteomics in driving the discovery of new biological insights and guiding drug discovery efforts.

Acknowledgements

Martje Erkelens is kindly acknowledged for performing the ALDEFLUOR assay, Alexander Bakker and Bogdan Florea for mass spectrometry analysis, Vera van der Noord for her advice and technical assistance with the cellular assays, Else Botter for her collaboration on performing the cellular assays, Lukas Wijaya and Sylvia Le Dévédec for performing and analysing the live cell imaging.

Experimental procedures

Biological methods

Cell culture. The breast cancer cell lines BT-20, HCC38, MCF7, MDA-MB-231, MDA-MB-468, SK-BR-3 and SK-BR-7 were grown in RPMI-1640 with stable glutamine and phenol red with 10% Fetal Calf serum, penicillin and streptomycin at 37 °C and 5% CO_2. Medium was refreshed every 2-3 days and cells were passaged twice a week. Cell lines were purchased from ATCC and were regularly tested for mycoplasma contamination. Cultures were discarded after 2-3 months of use.

Flow cytometry. Cells from the different cell lines were used in the logarithmic growth phase for analysis with flow cytometry. The ALDEFLUOR assay (Stemcell, Cologne, Germany) was performed according to manufacturer's protocol. Subsequently, cells were stained with CD24 APC (Clone ML5, 1:100), CD44 PE Cy7 (Clone BJ18, 1:800), CD133 PE/Dazzle 594 (Clone 7, 1:100, all Biolegend, London, United Kingdom). Just before acquiring, DAPI (Invitrogen, Bleiswijk, the Netherlands) was added as a live death stain (1:40.000). Samples were acquired on LSR-Fortessa X20 (BD Bioscience, Mountain View, CA, USA) and data was analysed with Flowjo software (Tree Star, San Carlos, CA, USA).

Cell viability and proliferation. Breast cancer cells were grown to 80% confluence in 10 cm plates. Cells were then seeded in a 96-wells plate depending on their rate of growth (BT-20: 12 k/well; MDA-MB-468 & SK-BR-3: 10 k/well; SK-BR-7 & HCC38: 8 k/well; MDA-MB-231: 4 k/well). For the SRB proliferation assay cells were also seeded on an extra plate to be able to determine the starting point protein content. Cells were allowed to adhere overnight and were then treated with vehicle (0.1% DMSO) or inhibitor NCT-505 (30 µM, 0.1% DMSO) in 100 µL RPMI medium. Cells were then incubated for 72 hours.

For the MTT viability assay another 100 µL of medium containing MTT (1 mg/mL) was added and the cells were incubated for another 4 hours. The medium was then removed and the formazan crystals were dissolved in 100 µL DMSO during 1 hour in the stove. The absorbance was then measured in a CLARIOstar Plus plate reader at 570 nm.

For the SRB assay cells were fixated by incubation with 30 µL 50% TCA for 1 hour at 4 °C. The plates were washed 5 times with water and dried. 60 µL 0.4% SRB was added and incubated for 30 minutes at room temperature. The plates were then washed another four times with acetic acid (0.1%) and dried. The SRB was dissolved by adding 150 µL Tris (10 mM) and incubating for 30 minutes at room temperature. Absorbance was then measured at 540 nm on a CLARIOstar Plus plate reader. Graphpad Prism® 7 (Graphpad Software Inc.) was used to plot data and calculation of mean values and standard deviation.

Determination of ATP levels. MDA-MB-468 cells were seeded in 96-wells plates at 10 k/well. Cells were allowed to adhere overnight and were then treated with vehicle (0.1% DMSO) or inhibitor NCT-505 (30 µM, 0.1% DMSO) for 4 hour. The plate was then allowed to equilibrate for 30 minutes at room temperature. CellTiter-Glo assay (Promega) was then performed according to manufacturer's protocol. Measured on a CLARIOstar Plus plate reader and Graphpad Prism® 7 (Graphpad Software Inc.) was used to plot data and calculation of mean values and standard deviation.

Synergy of NCT-505 and RSL3. MDA-MB-468 cells were seeded in 96-wells plates at 10k/well. Cells were allowed to adhere overnight and were then treated with vehicle (0.1% DMSO), NCT-505 (3 µM, 0.1% DMSO), RSL3 (30 nM, 0.1% DMSO, Selleck Chemicals) or a combination of NCT-505 (3 µM) and RSL3 (30 nM). Cells were then incubated for 72 hours and a MTT assay was performed as described above. Graphpad Prism® 7 (Graphpad Software Inc.) was used to plot data and calculation of mean values and standard deviation. The IC28 values for both NCT-505 and RSL3 were calculated and used to determine the combination index value.

In situ activity-based proteomics

Sample preparation. Protocol adapted from previously described procedure.[31] Cells were treated *in situ*, harvested, lysed and adjusted to 1 mg/mL protein concentration as described above. 250 µL was taken from each sample and to this 25 µL freshly prepared "click" mixture containing 1 mM $CuSO_4$ (2.5 µL/sample, 100 mM in H_2O), 5 mM NaAsc (1.25 µL/sample, 1 M in H_2O), 0.4 mM THPTA (1 µL/sample, 100 mM in DMSO), 40 µM biotin-N_3 (2.5 µL/sample, 4 mM in DMSO) and MilliQ (17.75 µL/sample) was added. Samples were incubated for 1 hour at 37 °C while shaking (300 rpm). Excess click reagents were then removed by chloroform/methanol precipitation followed by another wash with methanol. Precipitated proteomes were then suspended in urea buffer (250 µL, 6 M urea and 25 mM ammonium bicarbonate), DTT (2.5 µL, 1 M) was added and the mixture was then incubated for 15 min at 65 °C while shaking (600 rpm). The samples were then allowed to cool down to RT and then alkylated by addition of iodoacetamide (20 µL, 0.5M) for 30 minutes at RT in the dark. Addition of SDS (70 µL, 10% (v/v)) was followed by heating at 65 °C for 5 minutes. For each sample 50 µL 50% slurry of Avidin-Agarose from egg white (Sigma-Aldrich) was washed three times with PBS and transferred in PBS (1 mL) to a 15 mL tube. To this another 2 mL of PBS was added followed by the corresponding proteome sample. The beads were incubated with the proteome for 2 hours at room temperature using an overhead shaker. The beads were then isolated by centrifugation (2 min, 2500 g), washed with SDS in PBS (0.5% (w/v)) and washed three times with PBS by centrifugation. The beads were then transferred to low-binding Eppendorf tubes and proteins were digested overnight at 37 °C and 950 rpm shaking in 250 µL digestion buffer (100 mM Tris, 100 mM NaCl, 1 mM $CaCl_2$, 2% acetonitrile and 0.5 µg sequencing grade trypsin (Promega)). Digestion was stopped by addition of formic acid (12.5 µL) and the beads filtered off by centrifugation (2 min, 600 g) using a Bio-Spin column (Bio-Rad). Samples were then desalted using stage tips, collected in low-binding Eppendorf tubes, concentrated using a SpeedVac (Eppendorf) and stored at -20 °C until reconstitution before measurement.[32] All samples were prepared in at least three biological replicates.

LC-MS/MS measurement and analysis. Samples were reconstituted in LC-MS sample solution (50 µL, MilliQ, 3% acetonitrile/0.1% formic acid/20 fmol/µL enolase). Samples were then analysed using a NanoACQUITY UPLC System (Waters) coupled to a SYNAPT G2-Si high-definition mass spectrometer (Waters) as previously described.[31,33] Of each sample 5 µL was loaded on a nanoEASE™ M/Z Symmetry C18 trap column (particles 5 µm, 100 Å , 180 µm x 20 mm, Waters) with 0.1% formic acid and separated on an nanoEASE™ M/Z HSS C18 T3 analytical column (particles 1.8 µm, 75 µm x 250 mm, Waters) heated at 80 °C. A multistep gradient running from 5-40% acetonitrile containing 0.1% formic acid during a 70 minute method at 300 nL/min was used to achieve peptide separation. Survey scans (m/z 50-2000 Da) were acquired in the Synapt with a scan time of 0.6 seconds in positive, resolution mode. The collision energy is set to 4 V in the trap cell for low-energy MS mode. For the elevated energy scan, the transfer cell collision energy is ramped using drift-time specific collision energies. The lock mass is sampled every 30 seconds. MS raw files were analysed with ProteinLynx Global SERVER (PLGS, v3.0.3, Waters). The MS^E identification was also performed with PLGS using the human proteome from Uniprot (uniprot-homo-sapiens-trypsin-reviewed-2016-08-29.fasta). The following parameter settings were used: low energy threshold 150 counts, elevated energy threshold 30, peptide and protein FDR 1%, enzyme specificity trypsin, max missed cleavages max 2, variable modification methionine oxidation, fixed modification carbamidomethylation cysteine, at least fragments/peptide 2, fragments/protein 5, peptides/protein 1 and number of peptides to measure per protein 3. For label-free quantification ISOQuant (v1.5) was used.[34,35] Data were filtered to retain only proteins with two or more reported unique peptides and quantified in at least 3 replicates of the positive control (probe-treated). Proteins were designated as significantly enriched by the probe when they showed 2-fold enrichment in quantification value when comparing negative control (vehicle-treated) with positive control (probe-treated) samples, probability as determined by a Student's *t* test (<0.05) and Benjamini-Hochberg correction with an FDR of 10%. The mass spectrometry proteomics data (raw data and IsoQuant output tables for proteins groups and peptides) have been deposited in the ProteomeXchange Consortium (http://proteomecentral.proteomexchange.org) via the PRIDE partner repository with the dataset identifier PDX015495.[36,37]

Heatmap ALDH profiles breastcancer analysis and correlation with transcriptomics and proteomics. Only ALDH enzymes significantly enriched in at least one breastcancer cell line (ALDH1A1, ALDH1A3, ALDH2, ALDH3A2) were selected for analysis. The mean raw LFQ intensities of triplicate measurements from two independent experiments were normalized using the LFQ mean raw LFQ intensity of the enolase internal standard and averaged. Average LFQ values for each ALDH enzymes were then calculated and used to determine the fold-change $\log_2$. The heatmap was prepared using Graphpad Prism® 7 (Graphpad Software Inc.). The $\log_2$ FC was plotted against transcriptomics and proteomics $\log_2$ FC data.

Breast cancer cell line mRNA microarray data used were previously established and are available in the Gene Expression Omnibus data repository (GEO) (accession number: GSE41313).[38] Protein abundance in the breast cancer cell lines was previously analysed using proteomics (manuscript in preparation, data available upon request).Transcriptomics data did not include the SK-BR-7 cell line. Linear regression and Pearson's correlation were calculated and plotted using Graphpad Prism® 7 (Graphpad Software Inc.).

In situ retinal conversion LC-UV/MS assay

Sample preparation. U2OS cells were grown in 6-wells plates and transiently transfected (N = 3). After 48 hours growth medium was replaces with medium containing retinal (30 µM) with serum. Cells were incubated for 4 hours, then washed with PBS and then PBS (1250 µL) was added. Cells were harvested using a cell scraper and then suspended in PBS. 1 mL of the suspension was moved to low-binding Eppendorf tube and 250 µL to a separate Eppendorf tube used to check for successful overexpression. The low-binding Eppendorf tube was spun down at 1000g for 5 min and then PBS was removed. Samples were snap frozen and stored at -80 °C until needed. A live/dead count was performed on the cells in the remaining Eppendorf tube after which cells were lyzed using a probe sonicator (5 sec, 30%). Samples were then denatured and loaded on gel, transferred to a membrane and the overexpression visualized using anti-FLAG antibody. When required low-binding Eppendorf tubes were thawed on ice after which acetonitrile (600 µL, LC-MS grade) was added. The cells were lyzed using a probe sonicator (5 sec, 30%) and spun down (14000 g, 5 min). The lysate was transferred to a new low-binding Eppendorf tube. Lysates were collected in low-binding Eppendorf tubes, concentrated using a SpeedVac (Eppendorf) and reconstituted in LC-MS sample solution (110 µL, 90% acetonitrile). Samples were vortexed, spun down (14000 g, 5 min) and transferred (100 µL) to a LC-MS vial after which they were measured.

LC-UV/MS measurement and analysis. Samples were injected onto a C18 column (50 x 4.6 mm, 3 µm; Nucleodur Gravity, Macherey-Nagel) connected to a Vanquish UHPLC system (Thermo Scientific) with a Vanquish Diode Array detector (Thermo Scientific) coupled to a LCQ™ Fleet (Thermo Scientific) via electrospray ionisation (ESI). Acetonitrile and water containing TFA (0.1%) were used for chromatographic separate of the retinoids. The solvent gradient was run from 10% acetonitrile for 1.5 min and then increased to 90% for 7.5 min. UV spectra were recorded between 200 and 600 nm. A calibration curve was made from a mix of retinoid standards (retinol, retinal, all-*trans* retinoic acid, 9-*cis* retinoic acid and 13-*cis* retinoic acid) measured at increasing concentrations (10 nM, 25 nM, 50 nM, 100 nM, 250 nM, 500 nM, 1 µM and 2 µM; N = 2, n = 4). Samples were then measured in duplo with a washing step after each sample. Quantification was performed using Xcalibur™ software (Thermo Scientific) after which the ratio between the UV spectra selected at 324, 356 and 380 nm were calculated for each peak to determine their purity. Concentrations were calculated using the calibration curve and averaged over the two measurements. The percentages of each retinoid as part of the total amount of retinoids detected in the samples were calculated.

Live cell imaging

Cell culture and lentivirus production. HEK293T cells were maintained in high-glucose Dulbecco's Modified Eagle Medium (DMEM, HyClone) with 5% fetal bovine serum (FBS, Gemini Bio) and 2 mM glutamine (Life Technologies) at 37 °C with 5% CO_2. To package lentivirus, HEK293T cells at ~70% confluence were transfected with pMDLg-RRE (gag/pol), pCMV-VSVG, pRSV-REV, and FUCCI plasmids (addgene#83841) using polyethyleneimine (PEI). Two days post-transfection, viral supernatant was filtered with a 0.45 µm polyethersulfone filter before using to infect the MDA-MB-468 cells.

Exposure and live cell imaging. Cells were seeded in Greiner black µ-CLEAR 96 well plates at 10k/well. Prior to the NCT-505 exposure, the cells were incubated with 100 ng/ml live Hoechst 33342 in complete RPMI for 2 hours. Thereafter, the medium was refreshed with complete medium. For cell death experiment, 0.2 µM propidium iodide (PI) and Annexin-V-Alexa633 (AnV) were added to the complete medium. For the live mitochondrial membrane potential imaging, the cells were incubated with rhodamine123 dye (0.5 µM; Sigma Aldrich) in combination with live Hoechst 33342 for 2 hours, thereafter we refreshed with complete medium containing rhodamine 123 only (0.075 µM) for time-lapse imaging. Then complete medium containing vehicle or NCT-505 (30 µM final concentration) was added and the plates were directly imaged onto the microscope stage for live cell imaging.

For the cell death experiment and mitochondrial membrane potential imaging, the plates were imaged at 0, 14, 24, 40, and 72 hours after the compound exposure. The cell cycle was imaged every hour after the exposure. The imaging was performed using a Nikon TiE2000 confocal laser microscope (lasers : 647 nm, 540 nm, 488 nm, and 408 nm), equipped with automated stage and perfect focus system. During the imaging, the plates were maintained in humidified atmosphere at 37 °C and 5% CO_2. The experiment was conducted with 3 biological replicates with 4-5 technical replicates.

Image analysis. The quantitative image analysis was performed with ImageJ version 1.52p, CellProfiler version 2.2.0 and Ilastik 1.3.2. Firstly, the nuclei per image were segmented using the watershed masked algorithm on ImageJ. For images obtained from the cell death and mitochondrial membrane potential experiment, the nuclear segmentation was performed with Ilastik 1.3.2. The images were processed with an in house developed CellProfiler module.[39,40] The images from the FUCCI cell line were analyzed and identified the object nuclei, geminin, and cdt with the IdentifyPrimaryObject module. The object geminin and cdt were masked with the segmented nuclei with the MaskImage module to eliminate the background. The cells expressing both proteins were identified as the yellow object by masking the images from the red channel with the geminin objects. The number of the nuclear object, geminin object, cdt object, and yellow object were counted as the outcome. For the cell death and mitochondrial membrane potential experiment , the nuclear Hoechst 33342 intensity levels, rhodamine 123 integrated intensity, PI area, and Annexin V area were measured at the single cell level. The results were stored as HDF5 files. Data analysis, quality control, and graphics were performed using the in house developed R package h5CellProfiler (manuscript in preparation).

Supplementary data

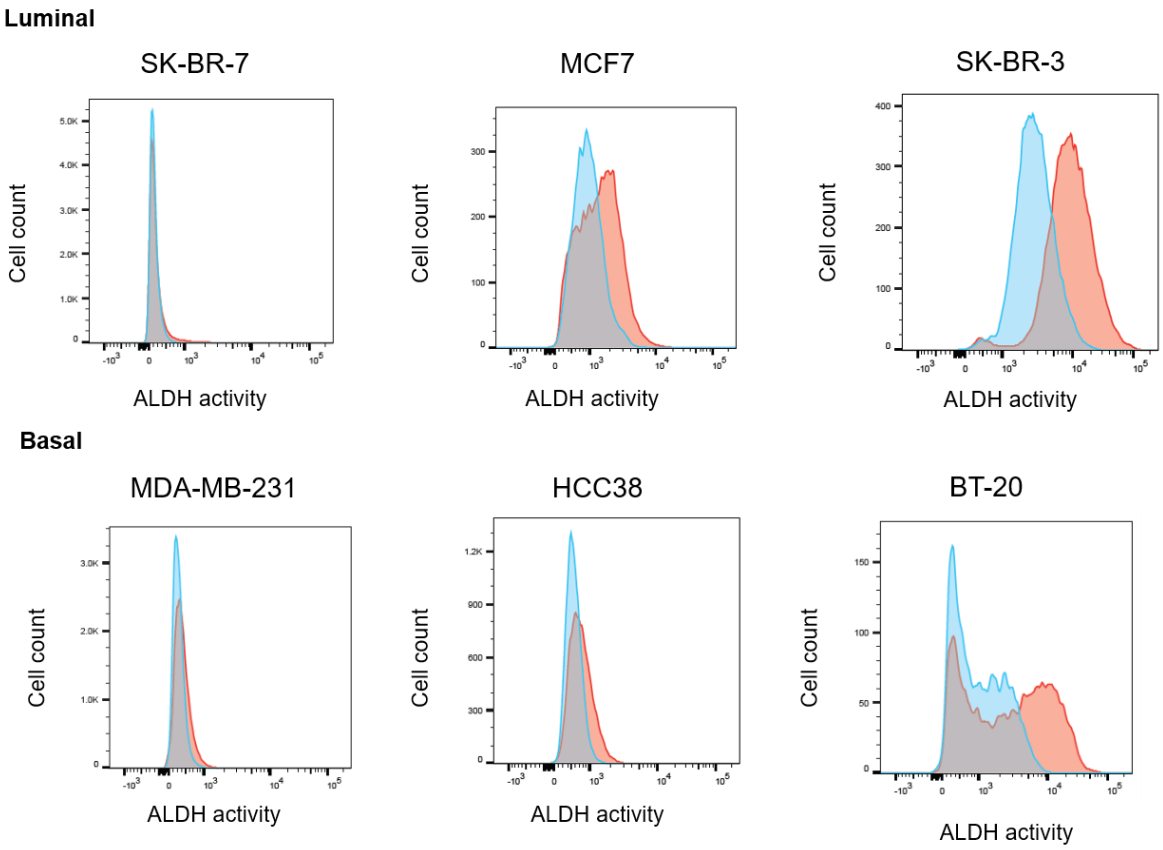

Supplementary Fig. 5.1 | Additional graphs for Figure 5.2a. Representative FACS plots of ALDEFLUOR assay in breast cancer cell lines. Cells treated with ALDEFLUOR (red) and a negative control in which cells were pre-treated with DEAB (blue).

References

1. Croker, A. K. & Allan, A. L. Inhibition of aldehyde dehydrogenase (ALDH) activity reduces chemotherapy and radiation resistance of stem-like ALDH hiCD44 + human breast cancer cells. *Breast Cancer Res. Treat.* **133**, 75–87 (2012).
2. Qiu, Y. *et al.* The expression of aldehyde dehydrogenase family in breast cancer. *J. Breast Cancer* **17**, 54–60 (2014).
3. Marcato, P. *et al.* Aldehyde Dehydrogenase Activity of Breast Cancer Stem Cells Is Primarily Due To Isoform ALDH1A3 and Its Expression Is Predictive of Metastasis. *Stem Cells* **29**, 32–45 (2011).
4. Sládek, N. E., Kollander, R., Sreerama, L. & Kiang, D. T. Cellular levels of aldehyde dehydrogenases (ALDH1A1 and ALDH3A1) as predictors of therapeutic responses to cyclophosphamide-based chemotherapy of breast cancer: A retrospective study. *Cancer Chemother. Pharmacol.* **49**, 309–321 (2002).
5. Tomita, H., Tanaka, K., Tanaka, T. & Hara, A. Aldehyde dehydrogenase 1A1 in stem cells and cancer. *Oncotarget* **7**, 11018–32 (2016).
6. De Beca, F. F. *et al.* Cancer stem cells markers CD44, CD24 and ALDH1 in breast cancer special histological types. *J. Clin. Pathol.* **66**, 187–191 (2013).
7. Luo, Y. *et al.* ALDH1A isozymes are markers of human melanoma stem cells and potential therapeutic targets. *Stem Cells* **30**, 2100–2113 (2012).
8. Zhou, L. *et al.* Identification of cancer-type specific expression patterns for active aldehyde dehydrogenase (ALDH) isoforms in ALDEFLUOR assay. *Cell Biol. Toxicol.* **35**, 161–177 (2019).
9. Koppaka, V. *et al.* Aldehyde Dehydrogenase Inhibitors: a Comprehensive Review of the Pharmacology, Mechanism of Action, Substrate Specificity, and Clinical Application. *Pharmacol. Rev.* **64**, 520–539 (2012).
10. Yasgar, A. *et al.* A High-Content assay enables the automated screening and identification of small molecules with specific ALDH1A1-Inhibitory activity. *PLoS One* **12**, 1–19 (2017).
11. Yang, S. M. *et al.* Discovery of Orally Bioavailable, Quinoline-Based Aldehyde Dehydrogenase 1A1 (ALDH1A1) Inhibitors with Potent Cellular Activity. *J. Med. Chem.* **61**, 4883–4903 (2018).
12. Koenders, S. T. A. *et al.* Development of a Retinal-Based Probe for the Profiling of Retinaldehyde Dehydrogenases in Cancer Cells. *ACS Cent. Sci.* **5**, 1965–1974 (2019).
13. Hollestelle, A. *et al.* Distinct gene mutation profiles among luminal-type and basal-type breast cancer cell lines. *Breast Cancer Res. Treat.* **121**, 53–64 (2010).
14. Storms, R. W. *et al.* Isolation of primitive human hematopoietic progenitors on the basis of aldehyde dehydrogenase activity. *Proc. Natl. Acad. Sci. U. S. A.* **96**, 9118–9123 (1999).
15. Wang, J. *et al.* Phosphorylation-dependent regulation of ALDH1A1 by Aurora kinase A: Insights on their synergistic relationship in pancreatic cancer. *BMC Biol.* **15**, 1–22 (2017).
16. Zhao, D. *et al.* NOTCH-induced aldehyde dehydrogenase 1A1 deacetylation promotes breast cancer stem cells. *J. Clin. Invest.* **124**, 5453–5465 (2014).
17. Yoshida, A., Hsu, L. C. & Dave, V. Retinal oxidation activity and biological role of human cytosolic aldehyde dehydrogenase. *Enzyme* **46**, 239–244 (1992).
18. Kang, J. H. *et al.* Aldehyde dehydrogenase is used by cancer cells for energy metabolism. *Exp. Mol. Med.* **48**, 1–13 (2016).
19. Burgos, C., de Burgos, N. M. G., Rovai, L. E. & Blanco, A. In vitro inhibition by gossypol of oxidoreductases from human tissues. *Biochem. Pharmacol.* **35**, 801–804 (1986).
20. Raha, D. *et al.* The cancer stem cell marker aldehyde dehydrogenase is required to maintain a drug-tolerant tumor cell subpopulation. *Cancer Res.* **74**, 3579–3590 (2014).
21. Sakaue-Sawano, A. *et al.* Visualizing Spatiotemporal Dynamics of Multicellular Cell-Cycle Progression. *Cell* **132**, 487–498 (2008).
22. Dixon, S. J. *et al.* Ferroptosis: An iron-dependent form of nonapoptotic cell death. *Cell* **149**, 1060–1072 (2012).
23. Hangauer, M. J. *et al.* Drug-tolerant persister cancer cells are vulnerable to GPX4 inhibition. *Nature* **551**, 247–250 (2017).
24. Viswanathan, V. S. *et al.* Dependency of a therapy-resistant state of cancer cells on a lipid peroxidase pathway. *Nature* **547**, 453–457 (2017).
25. Marcato, P., Dean, C. A., Giacomantonio, C. A. & Lee, P. W. K. Aldehyde dehydrogenase its role as a cancer stem cell marker comes down to the specific isoform. *Cell Cycle* **10**, 1378–1384 (2011).
26. Reynolds, D. S. *et al.* Breast Cancer Spheroids Reveal a Differential Cancer Stem Cell Response to Chemotherapeutic Treatment.

Sci. Rep. **7**, 1–12 (2017).

27. Fujiwara, D., Kato, K., Nohara, S., Iwanuma, Y. & Kajiyama, Y. The usefulness of three-dimensional cell culture in induction of cancer stem cells from esophageal squamous cell carcinoma cell lines. *Biochem. Biophys. Res. Commun.* **434**, 773–778 (2013).
28. Yang, W. S. *et al.* Regulation of ferroptotic cancer cell death by GPX4. *Cell* **156**, 317–331 (2014).
29. Schneider, C., Tallman, K. A., Porter, N. A. & Brash, A. R. Two distinct pathways of formation of 4-hydroxynonenal. Mechanisms of nonenzymatic transformation of the 9- and 13-hydroperoxides of linoleic acid to 4-hydroxyalkenals. *J. Biol. Chem.* **276**, 20831–20838 (2001).
30. Yoval-Sánchez, B. & Rodríguez-Zavala, J. S. Differences in susceptibility to inactivation of human aldehyde dehydrogenases by lipid peroxidation byproducts. *Chem. Res. Toxicol.* **25**, 722–729 (2012).
31. Van Rooden, E. J. *et al.* Mapping in vivo target interaction profiles of covalent inhibitors using chemical proteomics with label-free quantification. *Nat. Protoc.* **13**, 752–767 (2018).
32. Rappsilber, J., Mann, M. & Ishihama, Y. Protocol for micro-purification, enrichment, pre-fractionation and storage of peptides for proteomics using StageTips. *Nat. Protoc.* **2**, 1896–1906 (2007).
33. Distler, U., Kuharev, J., Navarro, P. & Tenzer, S. Label-free quantification in ion mobility–enhanced data-independent acquisition proteomics. *Nat. Protoc.* **11**, 795–812 (2016).
34. Distler, U. *et al.* Drift time-specific collision energies enable deep-coverage data-independent acquisition proteomics. *Nat. Methods* **11**, 167–170 (2014).
35. Kuharev, J., Navarro, P., Distler, U., Jahn, O. & Tenzer, S. In-depth evaluation of software tools for data-independent acquisition based label-free quantification. *Proteomics* **15**, 3140–3151 (2015).
36. Vizcaíno, J. A. *et al.* ProteomeXchange provides globally coordinated proteomics data submission and dissemination. *Nature Biotechnology* **32**, 223–226 (2014).
37. Perez-Riverol, Y. *et al.* The PRIDE database and related tools and resources in 2019: Improving support for quantification data. *Nucleic Acids Res.* **47**, 442–450 (2019).
38. Riaz, M. *et al.* MiRNA expression profiling of 51 human breast cancer cell lines reveals subtype and driver mutation-specific miRNAs. *Breast Cancer Res.* **15**, R33 (2013).
39. Wink, S., Hiemstra, S., Herpers, B. & van de Water, B. High-content imaging-based BAC-GFP toxicity pathway reporters to assess chemical adversity liabilities. *Arch. Toxicol.* **91**, 1367–1383 (2017).
40. Yan, K. & Verbeek, F. J. Segmentation for high-throughput image analysis: Watershed masked clustering. in *Lecture Notes in Computer Science (including subseries Lecture Notes in Artificial Intelligence and Lecture Notes in Bioinformatics)* **7610**, 25–41 (Springer, Berlin, Heidelberg, 2012).